Published in final edited form as:
Biomaterials. 2008 October ; 29(28): 3836–3846. doi:10.1016/j.biomaterials.2008.06.002.

The effect of silica nanoparticle-modified surfaces on cell morphology, cytoskeletal organization and function

Anna M. Lipski[a], **Christopher J. Pino**[b], **Frederick R. Haselton**[b], **I.-Wei Chen**[a], and **V. Prasad Shastri**[a,b,*]

[a] Department of Materials Science and Engineering, University of Pennsylvania, Philadelphia, PA 19104, USA

[b] Department of Biomedical Engineering, Vanderbilt University, Nashville, TN 37235, USA

Abstract

Chemical and morphological characteristics of a biomaterial surface are thought to play an important role in determining cellular differentiation and apoptosis. In this report, we investigate the effect of nanoparticle (NP) assemblies arranged on a flat substrate on cytoskeletal organization, proliferation and metabolic activity on two cell types, Bovine aortic endothelial cells (BAECs) and mouse calvarial preosteoblasts (MC3T3-E1). To vary roughness without altering chemistry, glass substrates were coated with monodispersed silica nanoparticles of 50, 100 and 300 nm in diameter. The impact of surface roughness at the nanoscale on cell morphology was studied by quantifying cell spreading, shape, cytoskeletal F-actin alignment, and recruitment of focal adhesion complexes (FAC) using image analysis. Metabolic activity was followed using a thiazolyl blue tetrazolium bromide assay. In the two cell types tested, surface roughness introduced by nanoparticles had cell type specific effects on cell morphology and metabolism. While BAEC on NP-modified substrates exhibited smaller cell areas and fewer focal adhesion complexes compared to BAEC grown on glass, MC3T3-E1 cells in contrast exhibited larger cell areas on NP-modified surfaces and an increased number of FACs, in comparison to unmodified glass. However, both cell types on 50 nm NP had the highest proliferation rates (comparable to glass control) whereas cells grown on 300 nm NP exhibited inhibited proliferation. Interestingly, for both cell types surface roughness promoted the formation of long, thick F-actin fibers, which aligned with the long axis of each cell. These findings are consistent with our earlier result that osteogenic differentiation of human mesenchymal progenitor cells is enhanced on NP-modified surfaces. Our finding that nanoroughness, as imparted by nanoparticle assemblies, effects cellular processes in a cell specific manner, can have far reaching consequences on the development of "smart" biomaterials especially for directing stem cell differentiation.

Keywords

Focal adhesions; F-actin fibers; Nanoroughness; Endothelial cells; Preosteoblasts; Nano-mechanotransduction

* Corresponding author. Department of Biomedical Engineering, 5824 Stevenson Center, Station B #351631, Vanderbilt University, Nashville, TN 37235, USA. Tel.: +1 615 322 8005; fax: +1 615 343 7919. prasad.shastri@vanderbilt.edu, prasad.shastri@gmail.com (V.P. Shastri).

1. Introduction

It is well established that a biomaterial's surface characteristics can alter cell behavior at many levels. Biological processes, such as differentiation, growth, and apoptosis, are arbitrated by cell shape and cytoskeletal organization directly determined by cell/surface interaction [1,2]. For example, DNA synthesis in a cell is closely coupled with cell spreading (i.e., shape of cell) on a surface [3]. The interaction of cells with a given material surface is dependent upon both surface texture (topography) and chemistry [4]. Micron sized features such as channels and ridges have been used to alter cell shape and alignment [5]. Many strategies have been explored to create micro and nanoscale topography on surfaces, such as lithography, chemical and plasma etching, grit blasting and plasma spraying, among others [6–9]. However, many chemical and topographical modification techniques are material specific, and are incompatible with cells and biological substrates. A new paradigm for nanoscale engineering of a biomaterial surface was recently reported [10]. In this paradigm, an assembly of silica nanoparticles (NP) is used to impart well-defined texture and roughness to a surface, which is varied by controlling the size of the NP. Furthermore, through *a priori* modification of the NP, both chemistry and topography (texture, roughness) of a biomaterial surface can be modified in a single step. An important attribute of NP-based surface modification is that the surface modification occurs independent of the bulk properties of the biomaterial and is equally suitable for modifying metal and polymer substrates [10]. The utility of silica NP in surface modification lies in the ease with which silica surfaces can be modified to bear a wide range of functional groups and biological moieties.

It has been shown that NP-modified surfaces can dramatically enhance the differentiation of human marrow derived mesenchymal progenitor cells towards an osteogenic lineage in the presence of soluble signaling molecules [10]. NP-modified surfaces, therefore, present a new paradigm for probing the effects of surface-bound information on cell shape and function, as the effects of texture and chemistry can be decoupled [10]. Secondary advantages of this strategy include control over surface roughness and surface area, ease of modification of non-planar macro-surfaces, and coating conditions that are compatible with biological substrates and proteins. In this paper we analyze the effects of silica NP assemblies on cell morphology through quantification of cell spreading, F-actin alignment and area of focal adhesions, in additional to functional metrics namely, proliferation and metabolic activity.

2. Materials and methods

2.1. Silica nanoparticle (NP) synthesis and characterization

Using the Stöber process, monodispersed silica NPs of three distinct mean diameters (50, 100 and 300 nm) were synthesized by varying the ratios of tetraethylorthosilicate (TEOS), ammonium hydroxide, and deionized water. All ethanol (EtOH) used for NP production was 200-proof (Fisher Scientific, Springfield, NJ, USA).

For NP synthesis, two solutions were prepared: one containing TEOS (Sigma-Aldrich, St. Louis, MO, USA) and EtOH, and the other composed of ammonium hydroxide, deionized water, and EtOH. Specifically, for the 50 nm NP, 4.2 g of TEOS was mixed with EtOH to a total volume of 50 ml. Next, a solution comprised of 2.5 g of ammonium hydroxide and 1.2 g of deionized water was made in EtOH (50 ml total volume). The ammonium–water–EtOH solution was slowly added to the TEOS–EtOH solution with stirring and the final mixture was further stirred overnight to allow for NP coarsening. The aforementioned procedure was also used to create the 100 and 300 nm NPs and the corresponding amounts of TEOS, ammonium hydroxide, and deionized water are listed in Table 1. NP size and polydispersity

were determined using dynamic laser light scattering (ZetaSizer 3000HS; Malvern Instruments Ltd., Malvern, UK). For each of the three different desired NP diameters, the reported light scattering values are the average ± standard deviation (SD) as shown in Table 1 and are representative of 10 different silica NP batches that were made. Additionally, for each batch of silica NP, the value that is calculated by the light scattering technique is in itself an average of 10 separate measurements.

2.2. Preparation of NP-modified glass substrates

The conditions for modifying surfaces with NP assemblies were optimized in an earlier study [10]. First, glass slides (Fisher Scientific, Springfield, NJ, USA) were manually cut using a diamond tip pen into squares approximately 1 cm^2, and ultrasonically cleaned for 5 min in hexane, acetone, ethanol, and deionized water, respectively, and oven-dried at 60 °C for 24 h prior to use. Before NP deposition, substrates were removed from the oven and allowed to cool for at least 1 h. Silica NPs were assembled via spin coating (Cost Effective Equipment, Brewer Science, Inc., Rolla, MO, USA). Specifically, 100 μl of the NP suspension was pipetted onto the surface, and the sample was spun at 2000 rpm for 20 s. This was repeated 10 times for each sample, allowing 1–2 min drying periods between depositions. Lastly, the silica NP-modified samples were heat treated at 80 °C for 2 h. The non-NP-modified glass slides were subjected to the same treatments and were used as experimental controls. Twenty four hours prior to cell seeding all experimental surfaces were sterilized by treatment with 70% ethanol for 20 min followed by overnight drying in a sterile laminar flow hood.

2.3. Characterization of NP-modified glass surfaces

Representative NP-modified glass substrates were characterized using scanning electron microscopy (SEM) and atomic force microscopy (AFM) and these data have been previously reported [10]. SEM images were obtained on a JEOL 6300FV microscope at an accelerating voltage of 10 kV and at a vacuum pressure of 3×10^{-6} torr. Additionally, during SEM, elemental composition of all surfaces was elucidated by energy dispersive X-ray spectroscopy (EDX/EDS).

AFM was used for the topographical contour mapping and roughness analysis of NP-modified surfaces. Surfaces were mapped in the tapping mode using a Multi-mode AFM (Digital Instruments, Santa Barbara, CA, USA) equipped with a prefabricated cantilever. A scan rate of 0.4–0.5 Hz was used, and all images were acquired at 512 sample points/line scan for maximum resolution. Images were captured and analyzed using Nanoscope® III software package provided by the manufacturer. All AFM images were obtained using the same cantilever and identical scanning conditions.

Surface roughness measurements, reported as the root-mean-square roughness (R_q) were carried out on images of randomly selected 1 × 1 μm regions. The R_q values reported represent an average of six measurements (three samples; two locations per sample that were at least several millimeters apart). Statistical differences between NP-modified surfaces and control surfaces were analyzed using paired *t*-tests in Excel, values are reported as the mean ± SD, and $p < 0.05$ was considered significant.

2.4. Cell culture

Culture media, trypsin, penicillin-streptomycin, and sodium bicarbonate were purchased from Invitrogen Corporation (Carlsbad, CA, USA). Fetal bovine serum was from HyClone (Logan, UT, USA). All other chemicals and products were from Sigma-Aldrich (St. Louis, MO, USA) unless otherwise stated. All cells were cultured in a humidified, constant temperature (37 °C) environment containing 5% carbon dioxide (CO_2).

Bovine aortic endothelial cells (BAEC) were harvested as previously described [11] provided by the laboratory of Keith Gooch, Ph.D. (Department of Biomedical Engineering, The Ohio State University, Columbus, OH, USA) and were cultured in Dulbecco's Modified Eagle Medium (DMEM), supplemented with 10% fetal bovine serum (FBS), and 1% penicillin-streptomycin (P/S), at 37 °C in a 5% CO_2. The absence of fibroblast contamination was verified visually. BAECs used in this study were between passages 3–9. Mouse calvarial preosteoblasts (MC3T3-E1) were purchased from ATCC (Manassas, VA, USA) and were cultured in alpha minimum essential medium (α-MEM) supplemented with 10% FBS, 1% P/S.

For all cell experiments in this study, cells were seeded on the sterilized NP-modified substrates, glass (Gl) and tissue culture polystyrene (TCPS) at an initial density of 3000 cells/cm^2, and were maintained in standard cell culture conditions (37 °C, 5% CO_2). In these studies both glass and TCPS served as positive controls.

2.5. Cell proliferation assay

BAEC and MC3T3 cells were seeded onto silica NP-modified, glass and TCPS surfaces and incubated over a 7-day period under standard cell culture conditions (37 °C, 5% CO_2). Media was replaced every other day of culture, and at the prescribed time points (24, 48, 96 and 168 h), and substrates were gently washed twice with PBS, then fixed with 4% paraformaldehyde (10 min), followed by another PBS wash (three times). Nuclei were stained using DAPI mounting medium from Vector Laboratories (Burlingame, CA, USA). Samples were stored in the dark at 4 °C until imaged.

The DAPI stained nuclei of cells were visualized with a Zeiss Axioplan2 microscope and the number of cells in a 3 × 3 mm grid at 100× magnification were counted manually. Two samples per surface and cell type were set aside for cell proliferation measurements, and the reported values are the mean ± SD.

2.6. Metabolic activity assay

Cell metabolic activity was assessed by thiazolyl blue tetrazolium bromide assay (MTT reagent, Sigma-Aldrich) [12]. BAEC and MC3T3 were seeded on unmodified glass, silica NP-modified glass substrates and TCPS surfaces, and on designated time points (24, 48, 96,168 h post seeding) the MTT assay was performed. Specifically, cultures were removed from the incubator and into the sterile laminar flow hood where the substrates were placed into new 12-well TCPS plates (one sample/well), and MTT solution (5 mg/ml made in RPMI-1640 without phenol red) was aseptically added to each well. Immediately after MTT addition, samples were incubated for an additional 4 h. Following the incubation period, MTT solution was gently aspirated from each well, and formazan crystals were dissolved by the addition of 1 ml/well of 0.1 N HCl (prepared in anhydrous isopropanol). The absorbance of each sample was measured at 570 nm using a BioSpec-1601 spectrophotometer (Shimadzu Corporation, Columbia, MD, USA). MTT experiments were carried out on three separate occasions, and in triplicate for each substrate tested (TCPS, glass (GL), 50,100, and 300 nm silica NP-modified surfaces) and cell types (BAEC and MC3T3-E1). All values are reported as the mean ± SD.

Paired Student *t*-tests were performed to determine statistical significance of growth and metabolic activity data (p values of ≤0.1) for each time point (24, 48, 96 and 168 h) by comparing the data at that given time point on 50, 100 or 300 nm NP surfaces to glass controls.

2.7. Immunohistochemical staining for vinculin and F-actin

Samples for cytoskeletal staining were prepared as follows. Cells were incubated on corresponding substrates (glass, NP-modified glass, and TCPS) for 24 h after seeding. Cells were then washed two times before fixation in 4% paraformaldehyde for 10 min, and then washed three more times to remove excess paraformaldehyde. Samples were then stored at 4 °C until staining for nuclei, F-actin, and vinculin, a protein associated with focal adhesion complexes (FAC).

Fixed samples were first permeablized with 0.1% Triton-X100 in PBS at room temperature for 7 min, washed two times with PBS, and in order to reduce nonspecific background staining samples were blocked with 10% bovine serum albumin (BSA) overnight. Between primary and secondary antibody incubation periods, as well as between F-actin staining and DAPI mounting, substrates were washed three times with 0.1% Triton-X100 (in PBS). All incubations were conducted at room temperature. After overnight blocking, BSA solution was aspirated and samples were first incubated for 1.5 h with primary antibody, followed by 1.5 h with secondary antibody, and 40 min with FITC-conjugated phalloidin.

After permeabilization, immunostaining for vinculin was achieved using a mouse anti-vinculin monoclonal primary antibody (1:100 dilution) and a goat anti-mouse IgG rhodamine-conjugated secondary antibody (1:200 dilution) from Chemicon International (Temecula, CA, USA). The cytoskeletal component, F-actin, was labeled following manufacturer's protocol using Alexa Flour 488 FITC-phalloidin from Molecular Probes, Inc. (Eugene, OR, USA). Lastly, cells were mounted using DAPI nuclear stain and samples were stored at 4 °C before imaging.

2.8. Image acquisition and analysis

2.8.1. Image acquisition—Single cells were imaged using the 40× objective on the Zeiss Axioplan2 microscope (Thornwood, NY, USA), and images were collected using Axiovision Rel. 4.2 software. A minimum of 50 cells per substrate were imaged and analyzed.

2.8.2. Image analysis

2.8.2.1. Cell area analysis: Cell areas were calculated using Scion Image program (Scion Corporation, Fredrick, MD, USA) by outlining the perimeter of the cell as visualized through F-actin staining. Values are represented in histograms in 500 μm^2 bin divisions. Bin divisions were chosen to visually represent the data such that the number of cells exhibiting certain ranges of areas corresponded with calculated values such as mean, median and mode, while also maintaining adequate precision to draw inferences about skewness. Skewness (sk), is a statistical measure that characterizes the degree of asymmetry of the distribution around its mean, wherein a perfectly Gaussian distribution has a sk of zero [13]. Negative sk values describe distributions with tail regions prior to the mean, and positive sk values refer to populations with tails in the numeric range greater than the mean. Large sk values denote distributions that have emphasis on extreme values, which vary the most compared to Gaussian distributions.

2.8.2.2. F-actin organization analysis: Staining for cytoskeletal F-actin allowed for the investigation of fiber alignment as a function of surface roughness and was carried out using Image Pro Plus Version 5 (Media Cybernetics, Silver Spring, MD, USA). Fiber alignment was defined as how closely the fibers in the cell aligned with the long axis of the cell, which was designated as the reference axis. For the calculation, the manual straight line measurement tool was used to trace each discernable fiber that was greater than 2 μm in length, and a reference line was drawn through the long axis of the cell. For each fiber,

Image Pro calculated an angle measure from the horizontal (x-axis) between −90 and 90°. For a measure of how aligned each fiber was with the long axis of the cell, a difference angle was calculated as the absolute value of the reference cell axis angle subtracted from each fiber angle (Fig. 1), where the difference angle = abs(β − α), which is an angle value between 0° and 90°. For all surfaces tested (glass and NP-modified) and cell type, 10 cells were analyzed, and values are represented in histograms in 5° angle bin divisions. In this analysis, fibers that exhibit alignment with the long axis of the cell have angles approaching zero.

2.8.2.3. Focal adhesion analysis: Focal adhesion complexes (FAC) were visualized through vinculin staining. FAC areas were analyzed using a Matlab (The MathWorks Inc., Natick, MA, USA) script. First, each image of vinculin stained cells was background corrected by using the background subtraction function. Then the images were thresholded and individual FAC clusters were identified and counted. Counts were also verified by manual inspection. Values are reported as means for the random analysis of 10 cells per NP substrate and cell type, plus or minus the standard deviation.

Focal adhesion areas of cells grown on NP-modified surfaces were statistically analyzed using SigmaStat (SPSS Inc., Build 3, Chicago IL, USA). As a first pass, a oneway analysis of variance (ANOVA) was used to determine the significance of the NP data sets. After passing, data from NP-modified surface groups were compared against data from the experimental control (glass surface) using the Holm–Sidak method to evaluate the significance of multiple experimental groups compared to controls [14].

3. Results

3.1. Characterization of NP-modified glass surfaces

The homogeneity and overall coating quality of the spun cast NP assemblies consisting of different sized NPs was verified using SEM and AFM. SEM imaging revealed spherical undulation due to the NP assemblies and imaging at various magnifications failed to reveal any discontinuities in the NP coating. The surface morphology and roughness information was obtained using AFM which demonstrated that by simply varying NP size, the surface topography on the nanometer length scale can be altered (Table 2). Furthermore, increasing NP size results in a corresponding increase in roughness values. Fig. 2 contains representative SEM and AFM images of NP-modified surfaces.

3.2. Cell spreading

Representative images of fixed and immunohistochemically stained BAEC and MC3T3 cells on various substrates are shown in Figs. 3 and 4, respectively. Fig. 5 shows histograms of cell areas (culture time, 24 h) for BAEC (Fig. 5A,C,E,G) and MC3T3 cells (Fig. 5B,D,F,H) as cultured on the different surfaces. Histograms were chosen to represent the cell area data on the corresponding nanorough surfaces as they provide information about the global distribution of the cell population, which cannot be fully represented by a single index, such as the mean or median. In general, BAEC cells are smaller in comparison to the MC3T3 cells, and this is borne out in the histograms with the majority of BAEC population exhibiting area between 1500 and 2500 μm^2 compared to 2000 and 4000 μm^2 for MC3T3. BAEC and MC3T3 cells also responded differently in terms of changes in cell area as a function of increasing roughness. BAEC cells tend to spread less with increasing roughness (larger NP size) as seen by the shift to smaller areas (Fig. 5). The mode of the distribution, as noted by the asterisk, shifts towards smaller areas when compared to glass. In contrast, MC3T3 cells responded by increasing their area of contact, as there is a shift right towards larger areas with increasing roughness when compared to glass. Furthermore, sk, which is a

statistical measure that characterizes the degree of asymmetry of the distribution around its mean, was calculated and is shown in the upper right-hand quadrant of each histogram in Fig. 5. The sk values confirmed the trend that was visually apparent in the histograms, namely that the two cell populations responded differently to the increase in roughness.

3.3. Cell proliferation

Cell density of both cell types, after 24 h, on all surfaces was similar, suggesting that the silica NP coating did not adversely affect the attachment and survival of the cells during the initial 24-h culture period (Fig. 6). An increase in the cell density (proliferation) was observed over the entire culture period (7 days) during which cell numbers were counted for both the BAEC and MC3T3 cell types on all surfaces tested (Fig. 6A,B, respectively). As can be seen from Fig. 6B, MC3T3 cells on 50 nm NP-modified surfaces exhibited higher cell numbers at all time points greater than 24 h when compared to those modified with 100 and 300 nm NP. Though this effect of roughness on cell density is not as evident in the BAEC cells, there is a marked difference in cell density on all time points >24 h for the surfaces modified with the 50 nm versus the 300 nm silica NP. This result is consistent with what was observed for the MC3T3 cells in that the cell density on the smaller silica NP-modified surface is greater than on the rougher, larger sized (300 nm) silica NP-modified surface.

3.4. Cell metabolic activity

One of the objectives of this study was to determine if nanoscale roughness affected cellular activity. To test this premise, the ability of live, metabolically active cells to reduce a tetrazolium salt, MTT, was measured. It was observed that nanoscale roughness influences the metabolic activity of the cell and is cell specific (Fig. 6C and D). Fig. 6C,D show the MTT activity per cell, normalized to TCPS for the BAEC and MC3T3 cell types respectively. This data confirmed that the NP surfaces were conducive to cell adhesion and proliferation (C and D). Additionally, the activity decreases at later time points, where the cells are close to confluence and proliferation is slowed by contact inhibition.

In Fig. 6C, the activity of BAEC grown on 300 nm NP is higher than BAEC grown on 50 or 100 nm NP surfaces. When taken together with cell density data, the trend of lower metabolic activity on a per cell basis suggests that the BAEC cells on 50 and 100 nm NPs reach contact inhibition and stasis more quickly than on the 300 nm NP-modified surfaces. BAEC on 300 nm NPs maintain elevated metabolic activity at the late time points of 96 and 168 h. The trend is also exhibited by MC3T3 cells in Fig. 6D; however, lower metabolism is more pronounced in MC3T3 on 100 nm NP than in MC3T3 on 50 nm NP. Once again, cells on 300 nm NP-modified surfaces maintain elevated metabolic activity at the later time points. Therefore, it is shown that by increasing surface roughness through modification with larger NPs (300 nm) that cell division was diminished in both BAEC and MC3T3 (Fig. 6A,B) over a 7-day period.

3.5. F-actin fiber organization

Micron sized surface features have been shown to cause alignment of F-actin stress fibers in adherent cells. To ascertain the effect of nanoroughness on F-actin distribution within a cell population, the orientation of the F-actin stress fibers with respect to the long axis of the cell was determined. A fiber was considered aligned if it exhibited an angle of 10° or less with respect to the long axis of the cell. The distribution of angles exhibited by F-actin fibers in cells cultured on various substrates is shown in Fig. 7; the percentage of aligned fibers is tabulated in Table 3.

The trend that emerges in both BAEC and MC3T3 cells is that introduction of NP assembly of increasing NP size, which results in an increase in surface nanoroughness, increases F-actin alignment. In BAEC a >50% increase in fibers exhibiting a high degree of alignment (angle ≤10° with respect to the long axis of the cell) is observed at all nanoroughness, while in the case of MC3T3, a 30–49% increase is observed on surfaces with nanoroughness (Table 3). This phenomenon is also apparent when looking at representative cell images in Figs. 3 and 4. The cells grown on unmodified glass substrates exhibit F-actin stress fibers, which emanate from the FAC in a radial fashion toward the nucleus. This has been previously described for cells grown on glass [15]. Interestingly, on NP-modified substrates of increasing NP size and increasing surface nanoroughness, the F-actin fibers begin to span the entire length of the cell, and FACs appear to localize at the cell periphery where the fibers terminate. This effect occurred in both cell types tested, however, it is even more pronounced in MC3T3 cells.

3.6. Formation of focal adhesion complexes (FAC)

FAC are structural points of contact between the cell and the substrate that associate with intracellular proteins and the F-actin cytoskeleton via transmembrane integrin components. Several studies have shown that integrins, when subjected to mechanical stresses, lead to rearrangements in the internal cytoskeleton (CSK), and these changes alter cellular biochemistry. Therefore it can be inferred that surface geometry and the length scale of the surface features may distribute stresses differently, resulting not only in fiber remodeling, but also changes in fiber density, which can in turn affect cell function. The average total area of FACs per cell, for each cell line and for each surface is shown in Fig. 8. While the effect of nanoroughness on FAC formation appeared to be cell type specific, some trends could be determined within a cell type. BAEC cells grown on NP-modified surfaces exhibited a smaller total combined area of FAC versusglass control. This was most pronounced on the 50 and 100 nm NP surfaces and less so on 300 nm NP surfaces. However, in the case of MC3T3 cells, NP-modified surfaces exhibited more FAC compared to MC3T3 on glass controls. This is most prominent for 100 and 300 nm NP-modified surfaces. An important correlation that became apparent was that cells with the smallest total FAC areas were those that had the greatest F-actin fiber alignment. For BAECs this occurred on surfaced modified with 100 nm NP and for MC3T3 this occurred on surfaces modified with 50 nm NP.

4. Discussion

Cell processes such as proliferation, apoptosis and differentiation, are directly affected by substrate interaction and cell morphology through mechanotransduction mediated by spatial distribution and aggregation of receptors in response to an external stimulus. Several researchers have demonstrated that the area and density of cell-substrate contacts can be impacted by micron scale features. In this study, we have shown these same parameters can be influenced by nanoscale texture (roughness) possessing periodically spaced features. To the best of our knowledge, this is the first report wherein a NP surface modification approach has been used to introduce nano-texture in a controlled and systematic fashion as a means to probe cell behavior. To study cell behavior on NP coated surfaces, we chose to use two very different cell types, BAEC and MC3T3-E1 cells, which were studied without G-phase synchronization, and in the presence of serum. The choice of these two cells was based on the following criteria: ease of obtaining pure cell populations, abundance of literature on these cell types, differences in cell size – (BAEC is smaller than MC3T3), and differences in motility – (BAEC is more migrationally active than MC3T3 in monolayers). Our goal of these *in vitro* studies was to gain insights into the global effects that are representative of an *in vivo* environment. Therefore, studies were conducted in the presence

of serum using cells that were not G-phase synchronized. An important observation from these studies was that cell proliferation is adversely affected by 300 nm NP surfaces for both cell types. Previous studies have also shown that surface roughness slows cell proliferation [16–22]. This suggests that there is a critical length scale in which cells process spatial information, which has a direct bearing on cell proliferation. Although G-phase synchronized cells might shed more insight into the effects of nanoroughness on cell-cycle progression, it is beyond the scope of this report and the subject of an ongoing study.

The observed effect of nanoscale roughness on F-actin assembly may be attributed to differential protein adsorption, FAC density and/or changes in cell membrane tension caused by underlying nanoroughness [23–25]. Since the current experiments were carried out in the presence of serum, and the substrates possess identical chemistry it is therefore reasonable to assume that the same plurality of proteins will be present on all surfaces in similar compositions. However, it is plausible that nano-textured surfaces may promote differential protein absorption by inducing conformational changes in proteins and providing an increased surface area [23,25,26]. This may be ruled out to be the dominant factor, on the basis that the dimensions of proteins are much smaller than the dimensions of the silica NP and therefore can be expected to cause no appreciable change to the nanoscale topography of the surface. In essence, the adsorbed serum proteins maybe thought of as a thin primer layer that while conforming to the surface topography, promotes cell attachment. BAEC and MC3T3 cell types both benefit from serum proteins, such as fibronectin, vitronectin, and laminin [27–29]. Based on this reasoning, one could eliminate changes in surface protein composition as the underlying cause for the observed cell behavior. Therefore, we conclude that the enhanced F-actin fiber alignment is the result of the NP-surface architecture, through FAC, which we will discuss further. In this scenario, the underlying surface nano-geometry alters the stresses exerted on the cell membrane through FAC, resulting in enhanced F-actin fiber alignment [23]. This reasoning is consistent with the observation that increasing NP size to 300 nm, which should increase the contiguous area of contact of the cell membrane with the underlying substrate, increases F-actin alignment and FAC area.

FAC are cytoskeletal components that play an important role in cell migration and division. The formation of FAC requires transmembrane translocation and lateral diffusion of proteins, processes expected to be altered by changes in membrane tension. The finding that FAC number are impacted in a cell specific manner suggests that nanoscale topography affects both cell membrane conformity (tension) and the way in which cells perceive and respond to these changes. This line of reasoning is consistent with the observation that FAC area is affected in more migrationally active BAEC. The decrease in FAC area in BAEC accompanies an increase NP imparted nanoroughness. As BAEC cells move across surfaces with nanoscale features, they may create fewer FAC, which is energetically favorable for movement, since FAC synthesis is energy intensive. It is reasonable to conclude that BAEC in order to move on the nanorough surfaces, compensate for fewer FAC by organizing longer F-actin strands that span the length of the cell body. Conversely, MC3T3 cells being less motile are more likely to create FAC. The absence of distinct lamellipodia on NP substrates in both cell types implies that locomotion on NP-modified substrates is arrested or slowed [30]. In contrast, formation of dendritic lamellipodia was observed for both cell types when cultured on unmodified glass substrates, which are associated with locomotion [31]. This is most evident with the BAEC cells. Furthermore, cells on the NP-modified surfaces fail to exhibit extension of lamellipodia and, hence, may exhibit diminished movement compared with cells on unmodified glass.

As mentioned earlier, a strong correlation was observed between FAC are a and F-actin fiber alignment in both cell types, with a decrease in FAC area favoring higher F-actin alignment. Interestingly, this occurred on surfaces modified with 100 nm NP in the case of BAEC and

50 nm NP in the case of MC-3T3. If the formation of points of anchorage, i.e. FAC, is critical for establishing tension within cells via F-actin cytoskeletal assembly, then one may conclude that larger nanoscale features may impact cell migration in a manner so as to favor this outcome.

BAEC cells are highly proliferative with doubling times in the order of 20 h, while MC3T3 cells proliferate more slowly with doubling times ranging from 38 h to 3 days depending on the substrate characteristics and culture conditions [15,32]. On average, the MTT activity in BAEC cells is about twice that of MC3T3 cells. Metabolic activity as assessed by the MTT assay is indicative of the total energy needs of a cell population, and is measured by mitochondrial dehydrogenase activity [21,33]. Though the reduction of MTT can be seen as a reliable marker of biochemical activity, it cannot be used as a marker to identify specific cell function [34]. Therefore, we cannot attribute the observed differences to a specific cell process. However, taken together with cytoskeletal data and proliferation data assessed by cell density, it appears that NP surfaces promote cell stasis and arrests locomotion, favoring conditions for differentiation.

Studies by Martin et al. have shown that primary chondrocytes expanded in the presence of FGF-2 retain their redifferentiation potential. They observed that expansion under FGF-2 impacted α-smooth muscle actin and F-actin stress fibers formation [35,36]. This study concluded that the absence of such alignment promotes a more elongated (anisotropic) cell morphology, which is more susceptible to redifferentiation upon exposure to exogenous biological signals. In this study, we find similar changes in the morphology of cells, in MC3T3 cells in particular, which is accompanied by increased F-actin alignment. This suggests the possible use of purely structural cues to induce changes in cell phenotype. In our own study using human marrow derived mesenchymal progenitor cells, we have shown that osteogenic differentiation in the presence of soluble osteoinductive factors, is enhanced by an order of magnitude on surfaces modified with NP assemblies [10]. These observations of this study taken in sum are consistent with some recent observations wherein mechanical stimulation and strain, and surfaces bearing disordered nanoscale topography have been shown to favor differentiated phenotypes in stem and mesenchymal cells [37–40]. However it is important to note that the cells used in this study are of animal origin and human cells may exhibit different behavior. Furthermore, studies with endothelial cells derived from microvasculature such as human umbilical vein endothelial cells should be carried out to gain further insight into how nanoroughness affects endothelial cell function due to differences in adhesion behavior. Also, the nature of the NP needs to be carefully selected based on the intended application. For example, cardiovascular applications would necessitate the use of polymeric NP as opposed to silica NP. We envisage that NP-induced nanoroughness can be easily implemented onto devices such as stents, neural prosthesis, and scaffolds to support cell growth through coating and electrostatic assembly strategies which is a subject of several ongoing studies in our laboratory.

5. Conclusions

The ability to control texture and biomolecular information at the biomaterial-tissue interface in a spatially controlled manner lends itself to nanoscale biomimetic engineering of biomaterial surfaces. In this study we specifically explored the effect of nanoroughness as imparted by colloidal silica NP assemblies on cell morphology, proliferation and cell metabolism. One of the major conclusions of this study is that nanoroughness does affect cell function at many levels but in a cell specific manner. Smaller surface features (50 nm) tend to favor cell proliferation in comparison to larger features (300 nm). Additionally, proliferation of cells on glass which has negligible roughness was comparable to that on 50 nm surfaces. An other important finding was that nanoparticle modification of surfaces

influences cytoskeletal assembly by promoting F-actin fiber alignment. With respect to cell morphology endothelial cells respond to increasing nanoroughness by reducing their area of contact, while the converse hold true for preosteoblasts. A similar trend in FAC formation was observed as well, with endothelial cells forming fewer FAC than preosteoblasts on nanorough surfaces in comparison to glass. These results taken together suggest that there exists a critical dimension of nanotopography for influencing cell function and that the threshold feature size for nano-mechanotransduction is cell specific. Surfaces modified with NP assemblies may provide a versatile platform for controlling cell proliferation, locomotion, and differentiation.

Acknowledgments

This work was supported in part by National Institutes of Health (R24 AI-47739-03) sub-award to VPS, an NSF IGERT Fellowship and an Ada I. Pressman Memorial Scholarship given by the Society of Women Engineers to AML, The Nanotechnology Institute, through the Ben-Franklin Technology Partners of Northeastern Pennsylvania, and graduate fellowship to CJP through National Institute of Health Vascular Training Grant (NIH HL 0775).

References

1. Boudreau N, Bissell MJ. Extracellular matrix signaling: integration of form and function in normal and malignant cells. Curr Opin Cell Biol 1998;10(5):640–6. [PubMed: 9818175]
2. Schwartz MA, Ginsberg MH. Networks and crosstalk: integrin signalling spreads. Nat Cell Biol 2002;4(4):E65–8. [PubMed: 11944032]
3. Folkman J, Moscona A. Role of cell shape in growth control. Nature 1978;273(5661):345–9. [PubMed: 661946]
4. Jayagopal, A.; Shastri, VP. Nanoengineering of biomaterial surfaces. In: Kumar, CS., editor. Nanotechnologies for the life sciences: cell, organ, and tissue engineering. Weinheim: Wiley-VCH; 2008. p. 461-505.
5. Ohara PT, Buck RC. Contact guidance in vitro. A light, transmission, and scanning electron microscopic study. Exp Cell Res 1979;121(2):235–49. [PubMed: 571804]
6. Flemming RG, Murphy CJ, Abrams GA, Goodman SL, Nealey PF. Effects of synthetic micro- and nano-structured surfaces on cell behavior. Biomaterials 1999;20(6):573–88. [PubMed: 10213360]
7. Itala A, Ylanen HO, Yrjans J, Heino T, Hentunen T, Hupa M, et al. Characterization of microrough bioactive glass surface: surface reactions and osteoblast responses in vitro. J Biomed Mater Res 2002;62(3):404–11. [PubMed: 12209926]
8. Nitschke M, Schmack G, Janke A, Simon F, Pleul D, Werner C. Low pressure plasma treatment of poly(3-hydroxybutyrate): toward tailored polymer surfaces for tissue engineering scaffolds. J Biomed Mater Res 2002;59(4):632–8. [PubMed: 11774324]
9. Wu MH, Park C, Whitesides GM. Generation of submicrometer structures by photolithography using arrays of spherical microlenses. J Colloid Interface Sci 2003;265(2):304–9. [PubMed: 12962664]
10. Lipski AM, Jaquiery C, Choi H, Eberli D, Stevens M, Martin I, et al. Nanoscale engineering of biomaterial surfaces. Adv Mater 2007;19(4):553–7.
11. Bourke BM, Roche WR, Appleberg M. Endothelial cell harvest for seeding vascular prostheses: the influence of technique on cell function, viability, and number. J Vasc Surg 1986 Sep;4(3):257–63. [PubMed: 3528533]
12. Mossman T. Rapid colorimetric assay for cellular growth and survival: application to proliferation and cytotoxicity assays. J Immunological Met 1983:55–63.
13. Mandrekar SJ, Mandrekar JN. Are our data symmetric. Stat Methods Med Res 2003 Dec;12(6): 505–13. [PubMed: 14653353]
14. Ludbrook J. Multiple comparison procedures updated. Clin Exp Pharmacol Physiol 1998 Dec; 25(12):1032–7. [PubMed: 9888002]

15. Augustin-Voss HG, Voss AK, Pauli BU. Senescence of aortic endothelial cells in culture: effects of basic fibroblast growth factor expression on cell phenotype, migration, and proliferation. J Cell Physiol 1993;157(2):279–88. [PubMed: 8227161]
16. Anselme K, Linez P, Bigerelle M, Le Maguer D, Le Maguer A, Hardouin P, et al. The relative influence of the topography and chemistry of TiAl6V4 surfaces on osteoblastic cell behaviour. Biomaterials 2000;21(15):1567–77. [PubMed: 10885729]
17. Boyan BD, Hummert TW, Dean DD, Schwartz Z. Role of material surfaces in regulating bone and cartilage cell response. Biomaterials 1996;17(2):137–46. [PubMed: 8624390]
18. Ingber DE. Tensegrity II. How structural networks influence cellular information processing networks. J Cell Sci 2003;116(Pt 8):1397–408. [PubMed: 12640025]
19. Kieswetter K, Schwartz Z, Hummert TW, Cochran DL, Simpson J, Dean DD, et al. Surface roughness modulates the local production of growth factors and cytokines by osteoblast-like MG-63 cells. J Biomed Mater Res 1996;32(1):55–63. [PubMed: 8864873]
20. Lincks J, Boyan BD, Blanchard CR, Lohmann CH, Liu Y, Cochran DL, et al. Response of MG63 osteoblast-like cells to titanium and titanium alloy is dependent on surface roughness and composition. Biomaterials 1998;19(23):2219–32. [PubMed: 9884063]
21. Maniotis AJ, Bojanowski K, Ingber DE. Mechanical continuity and reversible chromosome disassembly within intact genomes removed from living cells. J Cell Biochem 1997;65(1):114–30. [PubMed: 9138086]
22. Martin JY, Schwartz Z, Hummert TW, Schraub DM, Simpson J, Lankford J Jr, et al. Effect of titanium surface roughness on proliferation, differentiation, and protein synthesis of human osteoblast-like cells (MG63). J Biomed Mater Res 1995 Mar;29(3)
23. Curtis AS, Gadegaard N, Dalby MJ, Riehle MO, Wilkinson CD, Aitchison G. Cells react to nanoscale order and symmetry in their surroundings. IEEE Trans Nanobiosci 2004;3(1):61–5.
24. Webster TJ, Ergun C, Doremus RH, Siegel RW, Bizios R. Specific proteins mediate enhanced osteoblast adhesion on nanophase ceramics. J Biomed Mater Res 2000;51(3):475–83. [PubMed: 10880091]
25. Webster TJ, Schadler LS, Siegel RW, Bizios R. Mechanisms of enhanced osteoblast adhesion on nanophase alumina involve vitronectin. Tissue Eng 2001;7(3):291–301. [PubMed: 11429149]
26. Burridge K, Chrzanowska-Wodnicka M. Focal adhesions, contractility, and signaling. Annu Rev Cell Dev Biol 1996;12:463–518. [PubMed: 8970735]
27. Norris WD, Steele JG, Johnson G, Underwood PA. Serum enhancement of human endothelial cell attachment to and spreading on collagens I and IV does not require serum fibronectin or vitronectin. J Cell Sci 1990;95(Pt 2):255–62. [PubMed: 1695219]
28. Steele JG, Johnson G, McFarland C, Dalton BA, Gengenbach TR, Chatelier RC, et al. Roles of serum vitronectin and fibronectin in initial attachment of human vein endothelial cells and dermal fibroblasts on oxygen- and nitrogen-containing surfaces made by radiofrequency plasmas. J Biomater Sci Polym Ed 1994;6(6):511–32. [PubMed: 7532995]
29. Steele JG, Johnson G, Underwood PA. Role of serum vitronectin and fibronectin in adhesion of fibroblasts following seeding onto tissue culture polystyrene. J Biomed Mater Res 1992;26(7): 861–84. [PubMed: 1376730]
30. Eisenbarth E, Linez P, Biehl V, Velten D, Breme J, Hildebrand HF. Cell orientation and cytoskeleton organisation on ground titanium surfaces. Biomol Eng 2002;19(2-6):233–7. [PubMed: 12202188]
31. Small JV, Rottner K, Kaverina I, Anderson KI. Assembling an actin cytoskeleton for cell attachment and movement. Biochim Biophys Acta 1998;1404(3):271–81. [PubMed: 9739149]
32. Kennedy SB, Washburn NR, Simon CG Jr, Amis EJ. Combinatorial screen of the effect of surface energy on fibronectin-mediated osteoblast adhesion, spreading and proliferation. Biomaterials 2006;27(20):3817–24. [PubMed: 16563495]
33. Bassell GJ, Powers CM, Taneja KL, Singer RH. Single mRNAs visualized by ultrastructural in situ hybridization are principally localized at actin filament intersections in fibroblasts. J Cell Biol 1994;126(4):863–76. [PubMed: 7914201]

34. van Kooten TG, Whitesides JF, von Recum A. Influence of silicone (PDMS) surface texture on human skin fibroblast proliferation as determined by cell cycle analysis. J Biomed Mater Res 1998;43(1):1–14. [PubMed: 9509339]

35. Martin I, Suetterlin R, Baschong W, Heberer M, Vunjak-Novakovic G, Freed LE. Enhanced cartilage tissue engineering by sequential exposure of chondrocytes to FGF-2 during 2D expansion and BMP-2 during 3D cultivation. J Cell Biochem 2001;83(1):121–8. [PubMed: 11500960]

36. Martin I, Vunjak-Novakovic G, Yang J, Langer R, Freed LE. Mammalian chondrocytes expanded in the presence of fibroblast growth factor 2 maintain the ability to differentiate and regenerate three-dimensional cartilaginous tissue. Exp Cell Res 1999;253(2):681–8. [PubMed: 10585291]

37. Dalby MJ, Gadegaard N, Tare R, Andar A, Riehle MO, Herzyk P, et al. The control of human mesenchymal cell differentiation using nanoscale symmetry and disorder. Nat Mater 2007;6(12): 997–1003. [PubMed: 17891143]

38. Engler AJ, Rehfeldt F, Sen S, Discher DE. Microtissue elasticity: measurements by atomic force microscopy and its influence on cell differentiation. Methods Cell Biol 2007;83:521–45. [PubMed: 17613323]

39. Engler AJ, Sweeney HL, Discher DE, Schwarzbauer JE. Extracellular matrix elasticity directs stem cell differentiation. J Musculoskelet Neuronal Interact 2007;7(4):335. [PubMed: 18094500]

40. Kurpinski K, Chu J, Hashi C, Li S. Anisotropic mechanosensing by mesenchymal stem cells. Proc Natl Acad Sci U S A 2006;103(44):16095–100. [PubMed: 17060641]

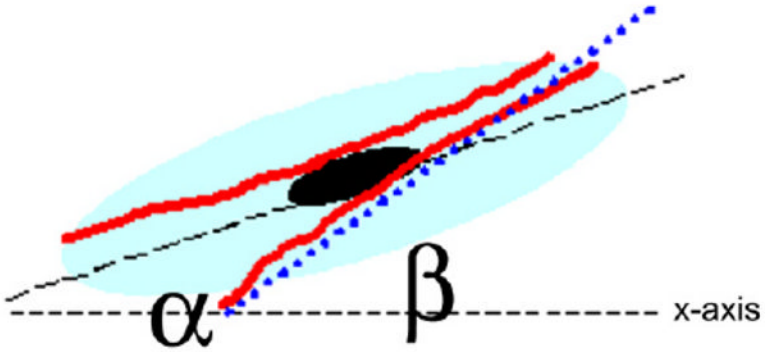

Fig. 1.

Schematic of F-actin fiber alignment calculation. Illustration represents the angles that were measured within the cell in order to carry out fiber alignment angle measurements. Fibers are shown in red; cell outline is shown in light blue and nucleus in black. Angle (α) is the angle that is formed between the x-axis and the long axis of the cell and angle (β) is the angle that is formed between the x-axis and the fiber.

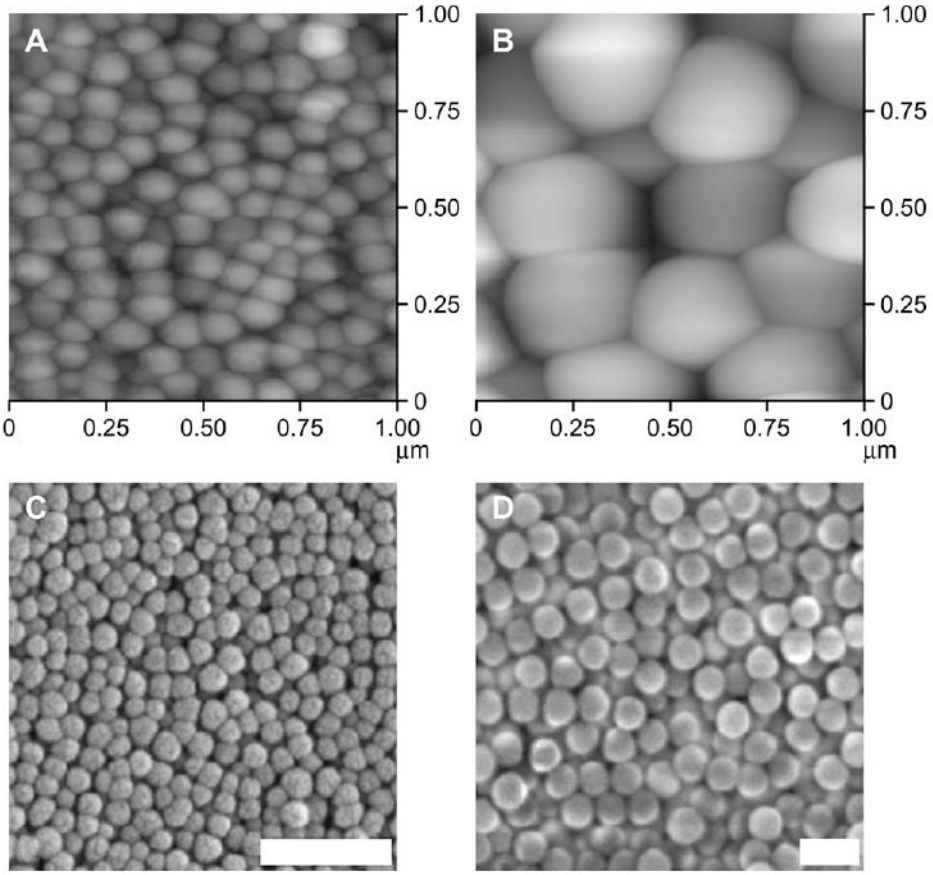

Fig. 2.

AFM and SEM characterization of 100 and 300 nm NP coatings on glass (Gl). **AFM:** (A) 100 nm silica NP-modified Gl; (B) 300 nm silica NP-modified Gl; **SEM:** (C) 100 nm silica NP-modified Gl; and (D) 300 nm silica NP-modified Gl. AFM images are 1 μm^2; scale bars on SEM micrographs are 500 nm. AFM and SEM of 50 nm NP were previously reported [10].

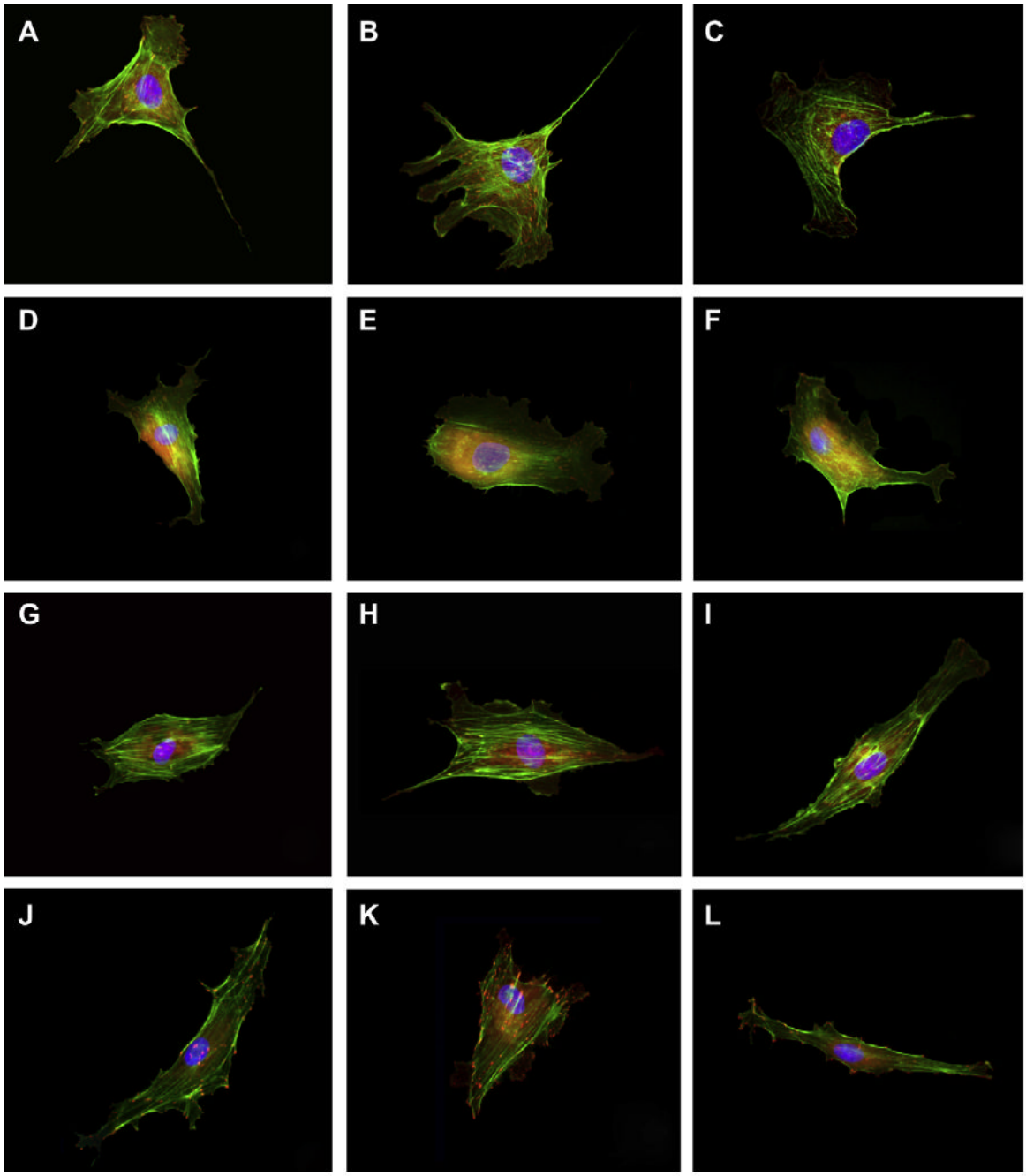

Fig. 3.

Representative images of BAEC cells cultured on NP-modified surfaces. Cells were fluorescently stained after a 24-h culture period for cytoskeletal F-actin fibers (green), FAC (red), and nucleus (blue). The substrates tested included: (A–C) unmodified glass; (D–F) 50 nm; (G–I) 100 nm; and (J–L) 300 nm silica NP-modified glass surfaces.

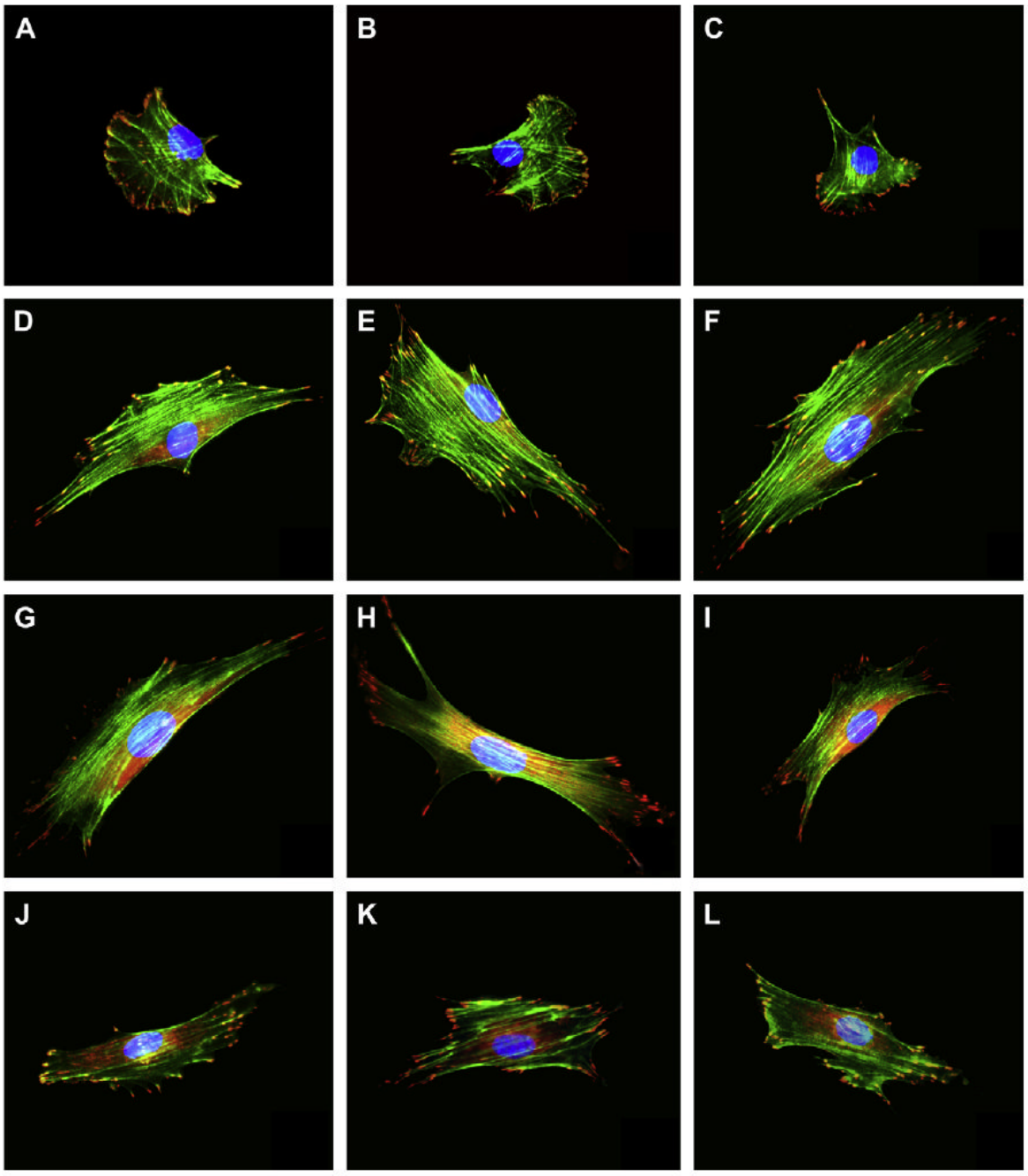

Fig. 4.

Representative images of MC3T3 cells cultured on NP-modified surfaces. Cells were fluorescently stained after a 24-h culture period for cytoskeletal F-actin fibers (green), FAC (red), and nucleus (blue). The substrates tested included: (A–C) unmodified glass; (D–F) 50 nm; (G–I) 100 nm; and (J–L) 300 nm silica NP-modified glass surfaces.

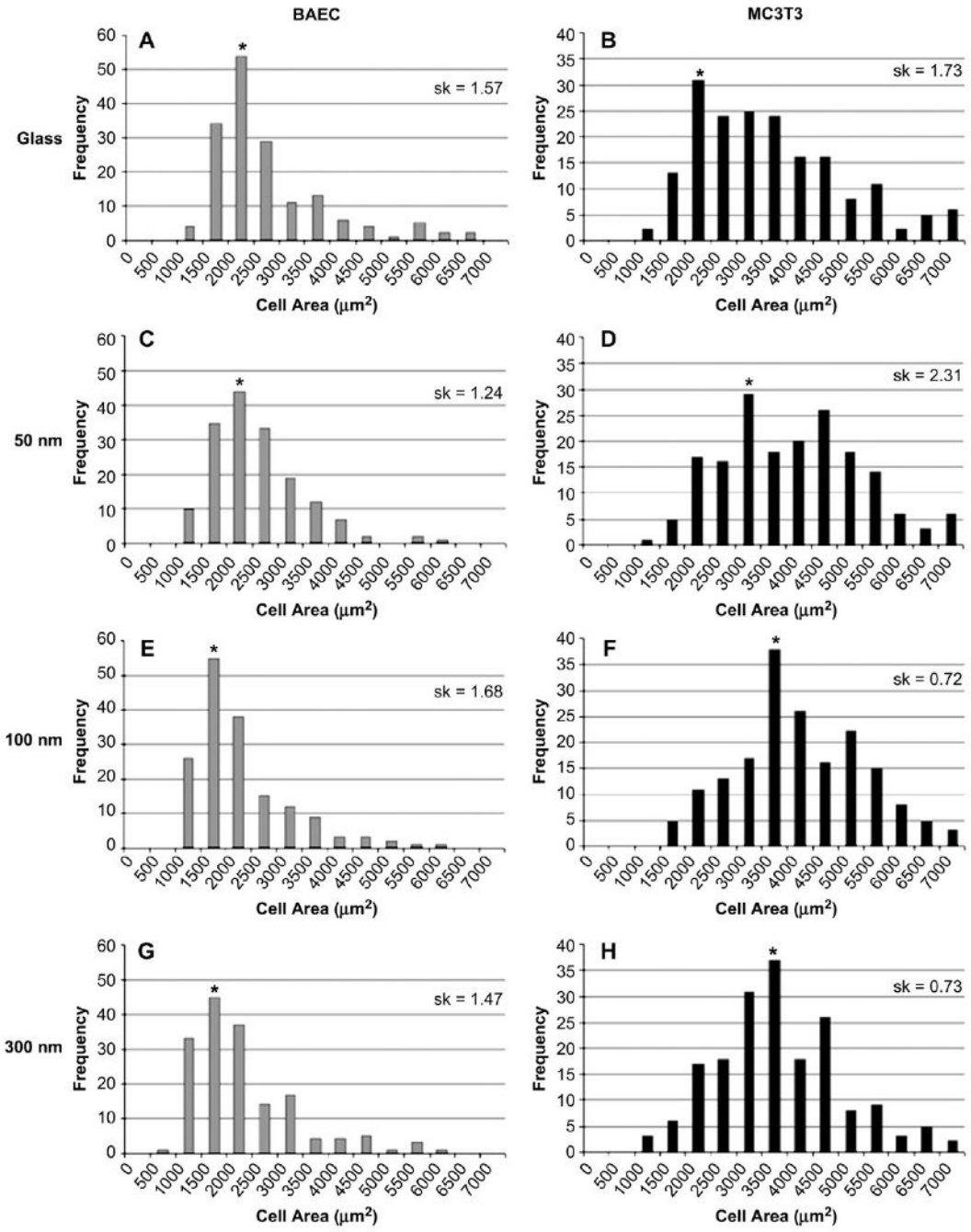

Fig. 5.

NP effect on cell area. Histograms represent cell areas after a 24-h culture period on the various substrates tested. A, C, E, and G are areas of BAEC cells; B, D, F, and H are areas of MC3T3 cells. Skewness (sk) for each population is reported in upper right-hand quadrant of the histogram and is determined using glass as the reference.

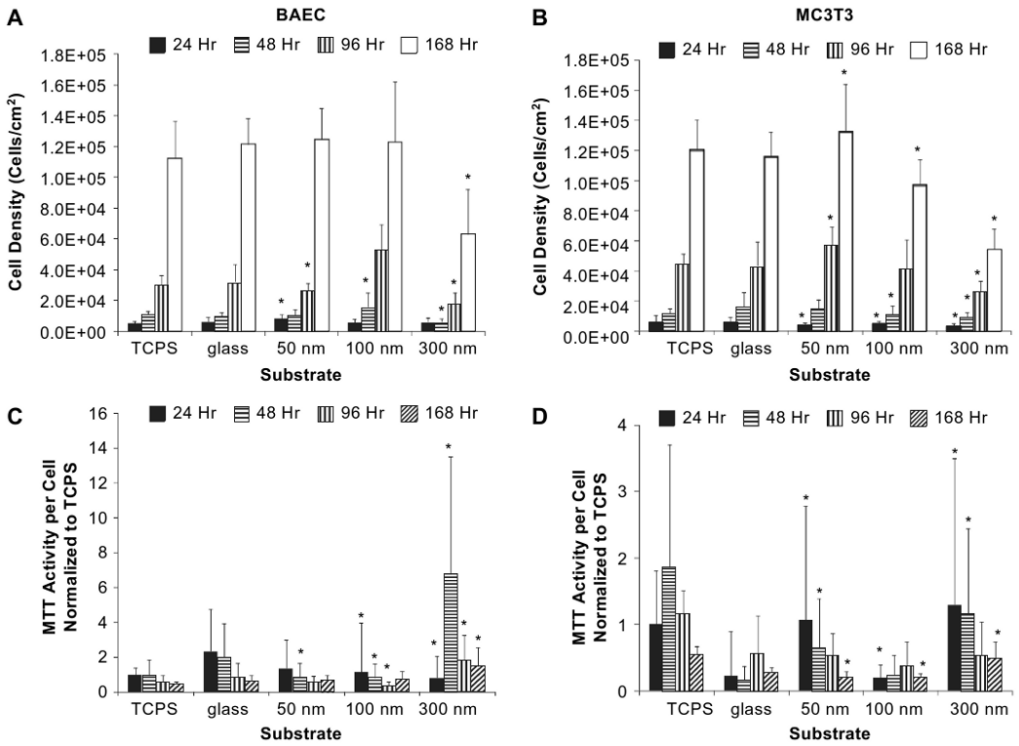

Fig. 6.

Mammalian cell proliferation and metabolic activity measurements. A and C represent BAEC data; B and D represent MC3T3 data. Metabolic activity (MTT) activity and cell number (density) were assessed over a period of 168 h (7 days). Initial seeding density was 3×10^3 cells/cm^2. Cell numbers were calculated for BAEC (A) and MC3T3 (B) is represented as values per unit area. MTT on a per cell basis and normalized to TCPS is shown in panel for (C) for BAEC and (D) for MC3T3. Asterisk represents data point that is statistically significant (p value of ≤0.1) in comparison to glass controls for that time point.

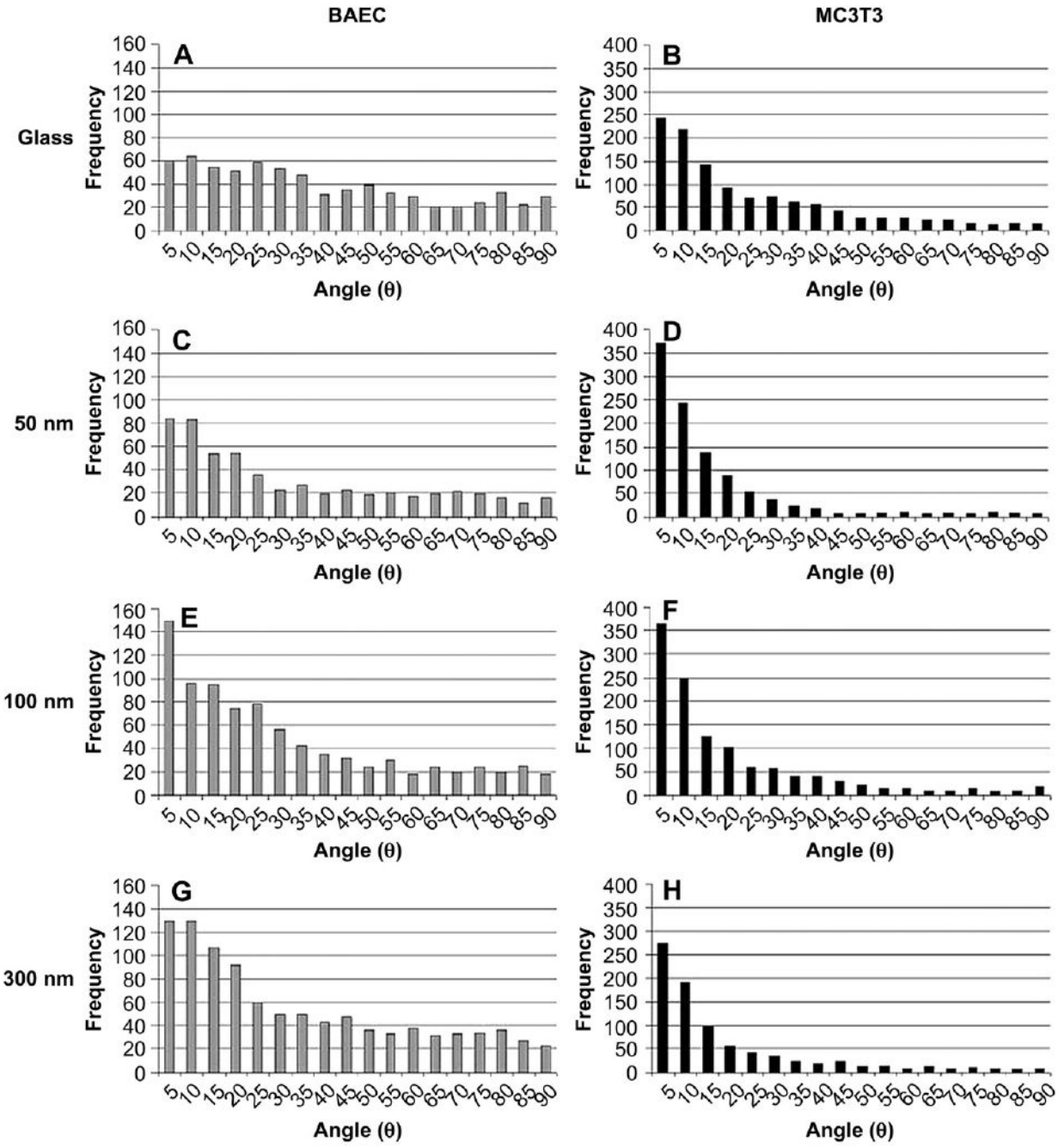

Fig. 7.

Effect of NP size on cytoskeletal F-actin alignment. Histograms represent cytoskeletal F-actin alignment (in degrees) with respect to long axis of cell. A, C, E, and G represent BAEC data; B, D, F, and H represent MC3T3 data. The substrates tested included glass, 50, 100 and 300 nm silica NP-modified glass surfaces.

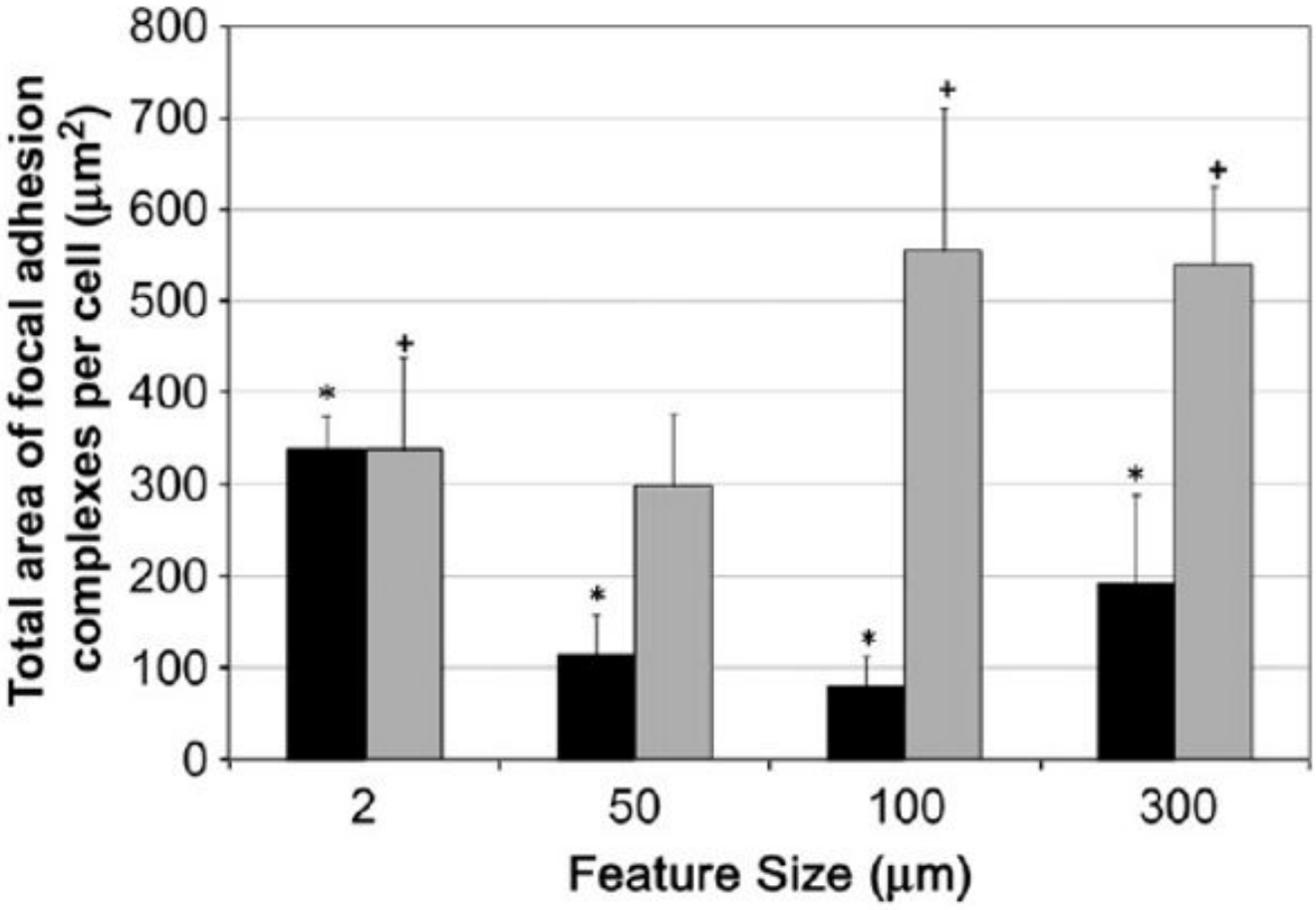

Fig. 8.

Focal adhesion complex (FAC) characterization of adherent cells on NP-modified surfaces and unmodified glass. FAC data for BAEC (black bars) and MC3T3 (gray bars) cells as cultured on glass, 50, 100 and 300 nm silica NP-modified glass surfaces. Total area of focal adhesion complexes per cell are reported as an average from 10 cells per NP substrate for each cell type. The feature size on glass surface is 2 nm. The asterisks (*) indicate statistical significance ($p < 0.05$) for all BAEC cultured on NP-modified surfaces when compared to the glass control. A plus (+) symbol indicates statistical significance ($p < 0.05$) for MC3T3 cultured on NP-modified surfaces when compared to the glass control.

Table 1

Reaction conditions for the preparation of silica NPs of various sizes

Desired size (nm)	TEOS (g)	Ammonium hydroxide (g)	Deionized water (g)	Average NP size (nm) as measured via laser light scattering	Average polydispersity index (PDI)
50	4.167	2.5	1.2	52.0 ± 2.96	0.06 ± 0.03
100	4.167	3.26	1.94	107.3 ± 6.3	0.02 ± 0.02
300	4.167	7.1	5.5	299.3 ± 7.7	0.06 ± 0.20

The corresponding sizes were measured via light scattering and values are the mean ± standard deviation.

Table 2

AFM surface roughness analysis

Substrate	R_q (nm)
Glass	0.2 ± 0.05
50 nm NP coating	2.44 ± 0.43
100 nm NP coating	20.44 ± 3.87
300 nm NP coating	69.38 ± 12.5

AFM surface roughness characterization of various sized silica NP coatings on glass substrates. Values are mean ± standard deviation of the root-mean-square roughness, R_Q, for silica NP coating assemblies.

Biomaterials. Author manuscript; available in PMC 2010 April 19.

Table 3

F-actin fiber alignment

A.					**B.**	
Cell type	**BAEC**		**MC3T3**		**BAEC**	**MC3T3**
Substrate	**<10°**	**<25**	**<10°**	**<25°**	**<10°**	**<10°**
Glass	17	41	39	64	–	–
50 nm NP coating	30	56	58	84	+68%	+49%
100 nm NP coating	29	57	52	77	+70%	+33%
300 nm NP coating	26	52	55	78	+52%	+41%

A. Percent of F-actin fibers exhibiting alignment within 10° and 25° of the long axis of the cell. Both BAEC and MC3T3 cells were cultured for a period of 24 h before fixing and staining. Unmodified glass, 50,100 and 300 nm silica NP-modified glass surfaces were tested. **B.** Percent increase in the number of F-actin fibers with alignment within 10° compared to glass surfaces.